

Reversible Switching of Battery Internal Resistance Using Iongate Separators

Matthew S. Gonzalez, Qizhang Yan, John Holoubek, Mingqian Li, Zhaohui Wu, Hongyao Zhou, Sean Kim, Haodong Liu, Bum-Young Jung, Suk-woo Lee, Zheng Chen, and Ping Liu*

Battery separators are a critical component that greatly determine cell calendar life and safety. Generally, these separators are passive with no ability to reversibly change their properties in order to optimize battery performance. Here, an iongate separator is demonstrated, which allows ion transport while in the oxidized “on” state but limits ion transport when switched to the reduced “off” state. This is achieved by depositing a dense 300 nm thin film of polypyrrole:polydopamine (PPy:PDA) on a conventional polyolefin separator. By using this iongate separator as a third electrode, a rapid and reversible order of magnitude increase of iongate resistance is achievable. The iongate battery shows similar cycling performance to a normal battery while in the “on” state, but cycling can be reversibly shut-off when the iongate separator is reduced to the “off” state. During elevated temperature storage with the iongate separator in the “off” state, battery capacity loss is decreased by 37% and transition metal crossover is greatly suppressed when compared to a normal battery without the iongate. Additionally, rapid shut-off during discharge is demonstrated by directly shorting the iongate separator to the anode.

reactive electrode materials and extreme operating conditions often required for these applications can result in faster battery degradation^[6] and increasingly energetic failure events.^[7]

For one, self-discharge and calendar life loss must be paid close attention to in large-scale and electric vehicle (EV) ESSs, particularly when operating under elevated temperatures.^[8,9,10] The two primary degradation mechanisms during storage are the parasitic oxidation reactions of the electrolyte at the cathode surface, where Li⁺ can then reintercalate into the cathode upon combination with liberated electrons,^[11] and dissolution of cathode transition metal ions into the electrolyte, which then crossover to and are reduced by the anode.^[12] The compromised solid electrolyte interface (SEI) then consumes more active charges in order to self-repair. This results in lost capacity

1. Introduction

Over the past three decades, lithium-ion batteries (LIBs) have fundamentally changed society by enabling portable consumer electronics.^[1] Within the next three decades, LIB price (\$ kWh⁻¹) is projected to decrease by nearly 80%,^[2] while production is expected to increase 30% year-to-year.^[3] LIBs remain the leading candidates for vehicle electrification^[4] as well as grid-scale energy storage.^[5] The demand for increased energy density coupled with ever-developing applications that require energy storage systems (ESSs) continues to drive battery innovation and optimization. However, if left unaddressed, the more

from the cathode itself, generation of a thicker and more resistive SEI on the anode surface, and irreversible consumptions of total Li capacity available in the cell.^[6] Battery management systems can disconnect the electronic pathway between electrodes and selective ion barriers have been developed to suppress unwanted crossover,^[13,14] however, there remains no simple and reversible method to ionically isolate the two electrodes thereby avoiding this problematic crosstalk during storage.

Furthermore, extremely rapid self-discharge can occur in the event of an internal electrical short. This short can be the result of mechanical damage to the cell or from an internal defect while operating under normal conditions.^[15] These short circuits can result in dangerous thermal runaway as evident by the recent ignition of EV's battery packs^[16] or the Boeing Dreamliner aircraft's auxiliary power unit forcing multiple emergency landings.^[17] During these severe shorting events, rapid self-discharge and Joule heating can quickly raise temperatures above the melting point of the separator and begin decomposing the electrode materials (150–250 °C), in turn triggering a chain of exothermic reactions and thermal runaway.^[18,19] The use of lithium metal anodes, the demand for rapid charging, and ever thinning separators all increase the likelihood of dendrite growth and other defect-induced shorting in addition to increased risk from mechanical deformation. To improve safety performance of high energy density cells, current collectors

M. S. Gonzalez, Q. Yan, J. Holoubek, M. Li, Z. Wu, Dr. H. Zhou, S. Kim, Dr. H. Liu, Prof. Z. Chen, Prof. P. Liu
Department of Nanoengineering
University of California San Diego
9500 Gilman Drive, La Jolla, CA 92093, USA
E-mail: piliu@eng.ucsd.edu

Dr. B.-Y. Jung, Dr. S.-w. Lee
LG Energy Solution Research Park
188, Munji-ro, Yuseong-gu, Daejeon 305-738, Republic of Korea

 The ORCID identification number(s) for the author(s) of this article can be found under <https://doi.org/10.1002/adfm.202102198>.

DOI: 10.1002/adfm.202102198

have been designed to fracture upon mechanical deformation,^[20] or with thermoresponsive polymers to electrically isolate active materials in an attempt to reduce the severity of failure events.^[21] Numerous flame-retardant,^[22,23,24,25] overcharge protection redox shuttle,^[26] or even shear thickening^[27] electrolyte additives have been developed to greatly improve battery safety; unfortunately, these are often electrochemically unstable at high voltages and sacrifice overall cell energy density.

The battery separator is a critical component that can be innovated to address these calendar life and safety challenges. Ideally, the separator should function as a reversible ion gate. Ion transport should be shut off during long-term storage or in the event of an internal short. Conversely, ion transport should remain on during charge and discharge. Most of the separator designs lack this reversibility. For example, many common battery separators go through nonreversible pore collapse at elevated temperatures, which eliminates ion flux between the electrodes before thermal runaway begins.^[28] Recently, more advanced features in separators have emerged. One such separator with a metal mesh sandwiched between two porous polypropylene layers acting as a third electrode can detect dendrite penetration, but the design requires constant monitoring and does not actually prevent shorting.^[29] A similar trilayer separator with reactive nanoparticles sandwiched in the middle layer was shown to etch away hazardous Li dendrites thus increasing the time-to-failure. We have recently shown that a bilayer Janus separator where one side is coated with a partially electronically conductive can not only detect the onset of dendritic shorting, but also dramatically slow the rate of self-discharge with minimal temperature rise during severe shorting events.^[30]

2. Results and Discussion

To this point, safety design has been largely focused on controlling the electronic pathway, making it very desirable to develop a novel method that allows reversible and dynamic control of the ionic conductivity of a cell. If ion flux could be temporarily shut-off during storage, so should the self-discharge and ion crossover while inherently improving safety. Additionally, having a mechanism that is electrochemically activated rather

than thermally triggered does not require temperatures to reach dangerous levels before initiating safety features.

Here, we improve battery control and safety by developing an iongate separator that exploits the switchable ionic conductivity exhibited in the conducting polymer polypyrrole (PPy) (Figure 1). By depositing a polypyrrole membrane on a conventional polyolefin separator, it is possible to fabricate an “iongate separator” that displays low ionic resistance while in its oxidized “on” state, and high ionic resistance while in the reduced “off” state. This is achieved by the rapid and reversible redox state transition of PPy where Li^+ ions are conducted via mobile anion dopants along the PPy backbone while in the “on” state, but are blocked in the nonconductive “off” state as the ions are expelled upon reduction.^[31] In other words, the oxidized polypyrrole membrane can be converted from a polycationic exchange membrane to a more neutral state upon reduction, which if sufficiently dense, prevents ion crossover.^[32] We demonstrate this switching can be achieved by ex situ means using a potentiostat connected to a third iongate electrode or by directly shorting the iongate material to the anode. Previous reports show a PPy iongate electrode can successfully prevent transient ion crossover in aqueous solutions;^[32,33] however, the concept has never been demonstrated in organic electrolytes or in a battery configuration to the best of our knowledge.

Polypyrrole is a well-known battery and pseudocapacitor material owing to its high conductivity, chemical, and electrochemical stability.^[34] Within batteries, PPy has found use in modifying electrode surfaces to improve performance of both cathode^[35,36] and anode materials,^[37] and even as an electrode material itself.^[38,39] Additionally, electrochemical polymerization provides a simple and versatile method to conformally deposit PPy films in a variety of configurations and morphologies.^[40]

Unfortunately, PPy suffers from poor adhesion due to lack of strong intermolecular interactions between PPy and common electrode surfaces. Polydopamine (PDA) has found use as a stable adhesive polymer for a number of applications;^[41] specifically, recent reports found introducing dopamine (DA) during pyrrole (Py) electropolymerization dramatically improves adhesion while maintaining electrochemical properties.^[42,43] Using a ratio of 2:1 Py:DA during electrochemical deposition (Figure 2a) results in a well adhered polypyrrole:polydopamine

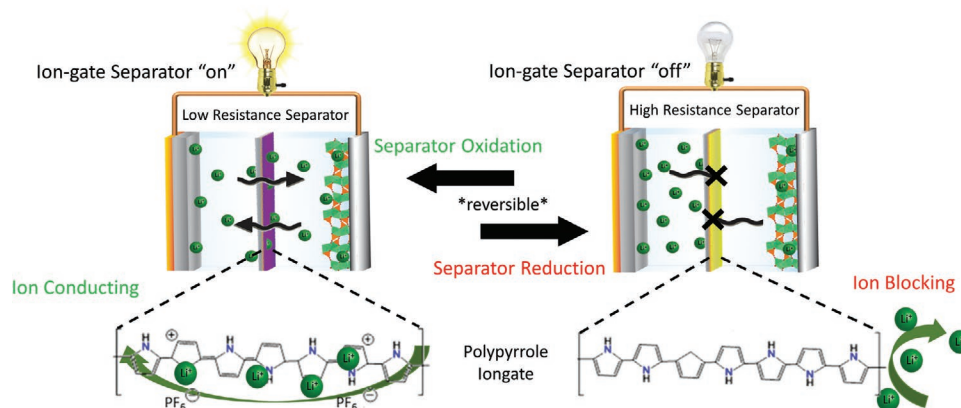


Figure 1. A schematic of the iongate separator in a low resistance oxidized “on” state and a high resistance reduced “off” state. While in the “on” state, Li^+ ions are conducted through the oxidized polypyrrole, whereas Li^+ ions are blocked by the reduced polypyrrole in the “off” state.

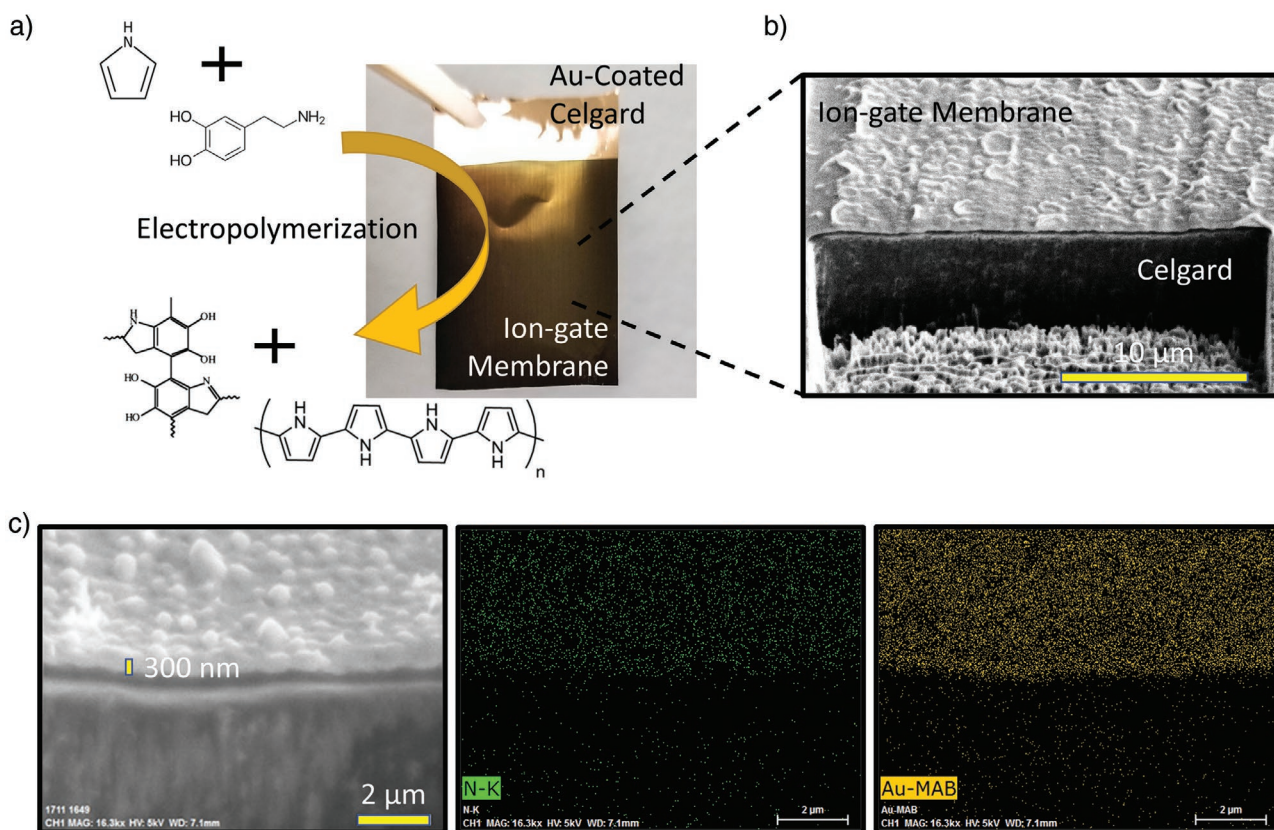


Figure 2. a) Polypyrrole:polydopamine (PPy:PDA) iongate membrane electropolymerization scheme and optical photograph of final iongate separator. b) Focused ion beam (FIB) cross-sectional SEM of iongate thin film polymerized directly on Au-coated Celgard. c) Higher magnification SEM/EDS elemental mapping showing the roughly 300 nm iongate film has not penetrated into the underlying separator. N is present in both the PPy and PDA, which cover the Au current collector to act as a third electrode.

(PPy:PDA) thin film on Au sputter-coated Celgard (Figure 2b). Higher magnification scanning electron microscopy/energy-dispersive X-ray spectroscopy (SEM/EDS) elemental mapping of the iongate separator cross-section (Figure 2c) shows the 300 nm PPy:PDA membrane, with N present in both the PPy and the PDA polymer, is conformally coated on and makes intimate contact with the underlay Au-coated Celgard without penetrating into the bulk of the Celgard. The Au coating was used as an electrochemically inert current collector^[29] for film deposition and in situ switching of the iongate material, and the coating process maintains the original porosity of the Celgard surface (Figure S1, Supporting Information). This Au coating layer is only ≈ 50 nm thick and has negligible contribution to the overall thickness of the separator.

An optimization of the membrane switching ratio versus thickness was performed and from this 300 nm was chosen as the final thickness (Figure S2, Supporting Information). As the layer becomes thinner, more pin holes form in the iongate due to underlying surface porosity of the Celgard substrate. This allows the liquid electrolyte to leak through an ideally dense iongate layer and decreases the reduced “off-state” resistance. When the iongate layer becomes too thick, the resistance in both the oxidized and the reduced state becomes much greater than that of a conventional cell without the iongate separator and hinders battery operation at realistic current densities.

The deposition process for this film requires only 3 min using a simple potentiostatic deposition method (0.65 V vs Ag^+/AgCl) and occurs in a relatively nonhazardous aqueous solution containing 0.1 M Py, 0.05 M DA, and 0.1 M LiTFSI as the dopant ion (Figure S3, Supporting Information). Raman spectroscopy confirms the copolymerization of PPy:PDA and matches previous reports describing the copolymerization of PPy and PDA (Figure S4, Supporting Information).^[43]

Additional iongate membranes were deposited with and without DA (Figure S5, Supporting Information). SEM shows clear delamination from the Au-coated Celgard without the addition of DA. Furthermore, various ratios of Py:DA were also examined (Figure S6, Supporting Information), where the higher the ratio of DA was shown to improve mechanical adhesion; however, above a 1:1 monomer ratio, an undesirable porous morphology was observed. The 2:1 ratio results in the most desirable dense morphology required for the iongate. Further details can be found in the Experimental Section.

Due to the hydrophilic nature of PDA, the iongate separator exhibits exceptional wettability. The iongate membrane over the top of the hydrophobic polypropylene Celgard dramatically improves the overall wettability of the iongate separator when compared to a pristine Celgard separator (Figure S7, Supporting Information).

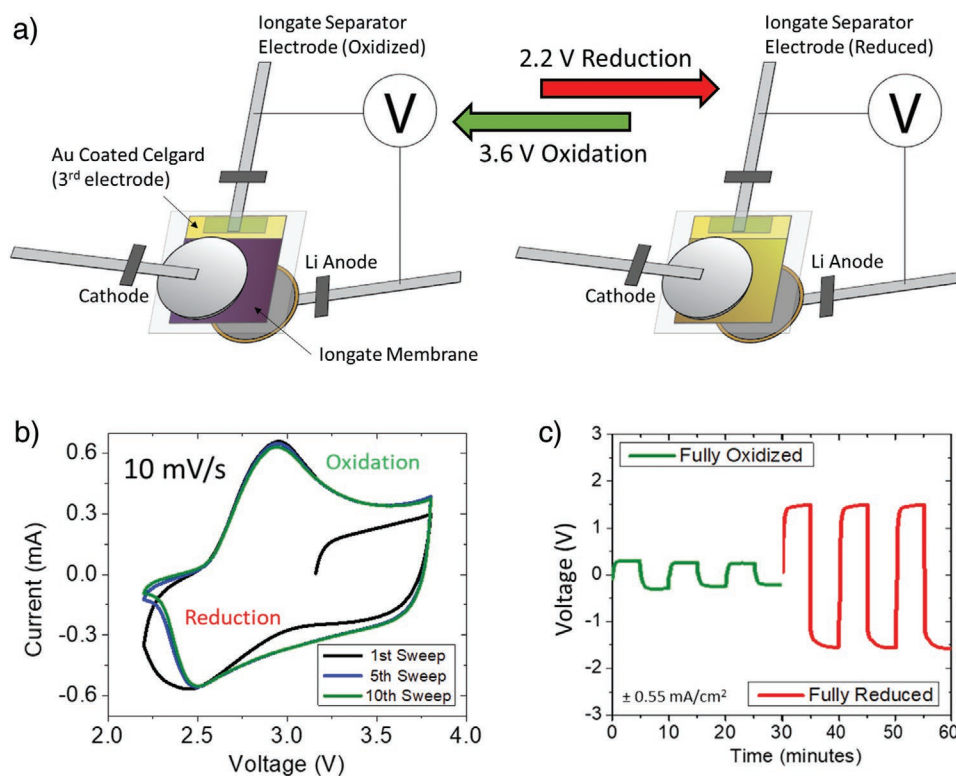


Figure 3. a) Schematic of three-electrode configuration for both Li/iongate/Li and Li/iongate/NMC cells where an additional contact is made to the iongate separator. Through this additional contact, various voltages can be applied to reduce (2.2 V) or oxidize (3.6 V) the iongate separator. b) Cyclic voltammetry of the iongate separator using a Li metal electrode as the counter and reference electrodes. c) DC voltage profile showing resistance switching between the oxidized “on” state and the reduced “off” state.

To measure the electrochemical performance of the iongate separators, a three-electrode cell was assembled in both Li/iongate/Li and Li/iongate/Li_xNi_{0.5}Mn_{0.3}Co_{0.2}O₂ (NMC) configurations as seen in Figure 3a. The potential of the iongate separator can be controlled through this third electrode contact to reduce or oxidize the iongate material. This is akin to discharging (reducing) and charging (oxidize) the iongate electrode, wherein discharging dedopes the PPy switching it to the “off-state” while charging redopes the PPy switching it to the “on-state.”

These cells used LP30 as the electrolyte (1 m LiPF₆ in ethylene carbonate:dimethyl carbonate (EC:DMC) 1:1 wt%). Pouch cells were fabricated to have an third electrode^[44] contact to the iongate separator through the exposed Au-coated Celgard remaining from the deposition process. An additional pristine Celgard was used to insulate the iongate membrane-coated side from the other electrodes—the backside of the separator remains pristine Celgard. Further details can be found in the Experimental Section.

Cyclic voltammetry (CV) of the iongate separator using the Li electrode as a counter and reference was performed to determine the redox properties. Two highly reversible redox peaks appear around 2.9 V for oxidation and 2.5 V for reduction using a scanning rate of 10 mV s⁻¹ (Figure 3b). There is a distortion during the 1st reduction compared to subsequent voltage sweeps likely due to expulsion of TFSI⁻ dopant used during deposition. Since the overall amount of PPy in the cell

is so small, less than 0.0005 m TFSI⁻ is expected to be in solution and should not result in significant change to the electrolyte. During the following oxidation PF₆⁻ from the bulk electrolyte is redoped into iongate membrane and the peaks remain stable and highly reversible as seen by the 5th and 10th voltage sweeps. With this information, 3.6 and 2.2 V were chosen as stable potentiostatic oxidation and reduction switching potentials for the follow across-membrane tests to ensure complete redox of the iongate.

The Li/iongate/Li configuration was used to measure the across-membrane DC resistance of the film in the oxidized “on” state and the reduced “off” state (Figure 3c). After the CV shown in Figure 3b, the iongate separator was held at 3.6 V for 30 min in order to ensure full oxidation of the iongate material. A DC square-wave current of ±1 mA (0.55 mA cm⁻²) was then applied across membrane and a resulting voltage polarization of roughly 250 mV was measured between the two Li electrodes. The iongate was next held at 2.2 V for 30 min to reduce the membrane, and again a current of ±1 mA was applied across membrane resulting in a voltage polarization of 1500 mV. From this data, the iongate areal resistance of the oxidized state and reduced state was determined to be 255 and 2443 Ω cm². These are calculated by subtracting off the average baseline resistance of 200 Ω cm² (i.e., a cell with only pristine Celgard (Figure S8, Supporting Information)) from the resistances measured in the iongate cell while in the on and off states to determine the added resistance of solely the iongate

separator, yielding a reversible iongate switching ratio of nearly 10 \times .

Additional common battery electrolytes were tested to confirm the robustness of the iongate concept. Since the iongate is deposited in LiTFSI, a 1 M LiTFSI in 1:1 wt% EC:DMC electrolyte was first tested in the Li/iongate/Li configuration. This similarly exhibited nearly an order of magnitude switching ratio in the iongate material between the oxidized and reduced states. The validity in an ether-based electrolyte was also tested using 1 M LiTFSI with 0.5 M LiNO₃ in 1:1 1,3-dioxolane:dimethoxyethane. While still showing clear switching, the magnitude of switching was slightly less—roughly 5 \times —owing to increased “off-state” conductivity despite similar redox characteristics as seen by the cyclic voltammetry. Further optimization and better understanding of iongate/electrolyte swelling interactions may be required for these systems; regardless, it appears that the iongate concept can be applied to numerous electrolyte systems. Detailed results can be found in Figure S9 in the Supporting Information.

To better understand the doping (oxidation) and dedoping (reduction) process, which is critically important to iongate working mechanism, XPS was performed on an oxidized and reduced sample of the iongate separator (Figure S10, Supporting Information). The doping level of the TFSI⁻ counterion in the oxidized state was calculated using the XPS survey scan to be 23%, or roughly one dopant ion for every four repeat pyrrole units, indicating a highly dope material. The doping level is effectively 0% for the reduced state indicating full reduction of the iongate material.

We next evaluated the iongate separator as a barrier for dissolved transitional metal ions, a well-known challenge when lithium-ion batteries are stored at elevated temperatures.^[45] Here, we choose a Li/iongate/NMC configuration, hereafter referred to as “iongate battery” (Figure 4). A “normal battery” was also fabricated without the iongate separate (i.e., only pristine Celgard). Further details of the battery fabrication can be found in the Experimental Section. It should be noted that to ensure the iongate material was in a fully oxidized state before battery cycling, the iongate separator underwent cyclic voltammetry and a 30 min oxidation hold at 3.6 V, as performed in Figure 3. The cells were then cycled at a rate of C/20 between 2.7 and 4.5 V with a 4.5 V hold until current decayed to C/40 for the first two cycles and the third charge process. The iongate was then reduced using a 2.2 V hold and pinned to that potential for storage. Both cells were then stored in this fully charged state at 55 °C for \approx 2 weeks to promote ion dissolution and self-discharge^[46] while measuring open circuit potential (OCP) in storage (Figure S11, Supporting Information). The iongate cell measured a higher OCP throughout storage appearing to significantly suppress the initial potential decay by \approx 50 mV after 2 days and remained >10 mV higher after 14 days. Cells were returned to room temperature and the iongate was reoxidized using a 3.6 V hold for 30 min. After this aging process, the cells were then discharge using a rate of C/40 at room temperature and the remaining capacity from the previous charge was 96.4% and 94.3% for the iongate battery and the normal battery, respectively (Figure 4a,d). This equates to a capacity loss reduction of \approx 37%. This noticeable improvement in capacity

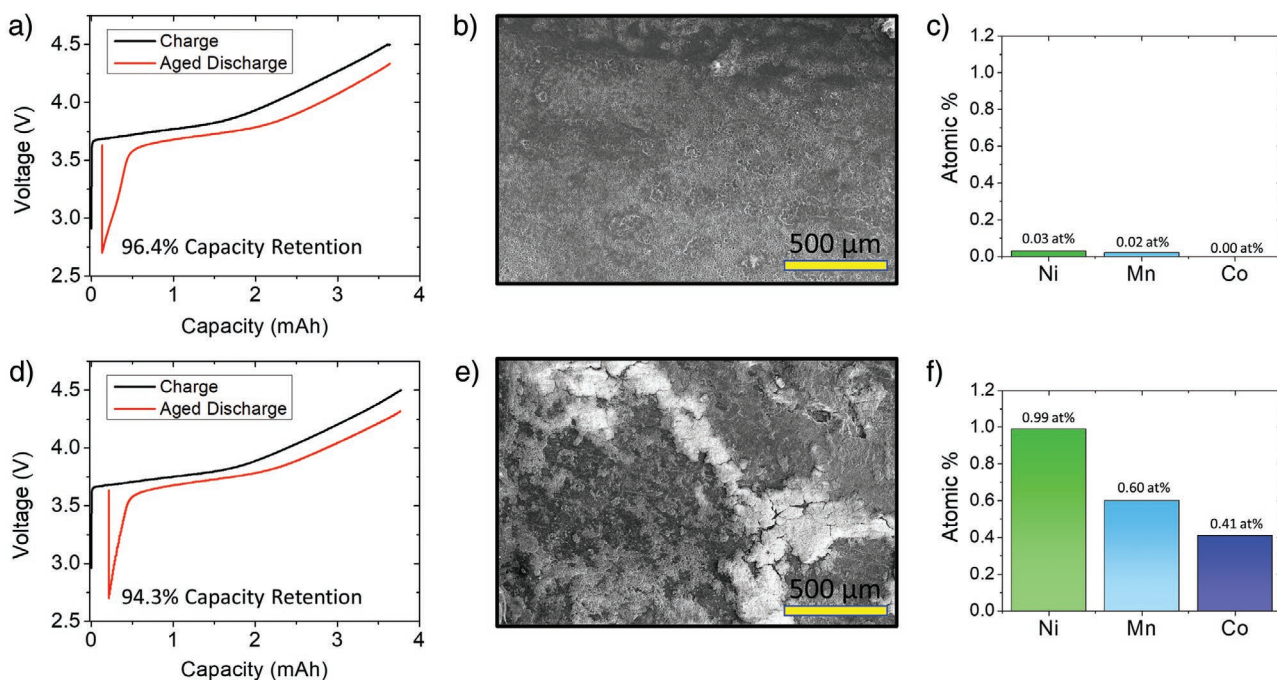


Figure 4. a) Charge and subsequent aged discharge profile of a battery with an iongate separator after being stored in the charged state for 2 weeks at 55 °C. During storage, the iongate separator was reduced, placing the battery in an “off-state” to limit spontaneous ion crossover and self-discharge. b) SEM of the Li metal anode surface after the 55 °C storage and discharge showing a uniform and dense SEI layer, and c) EDS elemental survey of the shown area with almost no transition metals (i.e., Mn, Co, Ni) detected. d) Charge and subsequent aged discharge profile of a normal battery without an iongate separator stored in the same conditions. e) SEM of the Li metal anode surface after the 55 °C storage and discharge showing a very nonuniform SEI that greatly varies in thickness. f) The EDS elemental survey of this area with a significant amount of transition metals detected.

retention is attributed to the reduced state iongate's ability to largely limit the crossover of ions across the separator during high temperature storage.

Our hypothesis is supported by the difference in morphology and chemical composition of the SEI formed on the Li metal anode surface during storage. After the final discharge, both cells were disassembled, and the Li metal anodes were gently washed using pure DMC solvent. SEM of the anode surface show two very different morphologies: The iongate battery anode has a relatively uniform and dense SEI (Figure 4b) whereas the normal battery anode SEI is very inhomogeneous with areas of greatly varying thickness (Figure 4e). It is well known that nonuniform SEIs are extremely prone to future dendrite growth due to irregularities in surface resistance and Li^+ ion flux.^[47] EDS elemental mapping for these anode areas (Figure S12, Supporting Information) show the iongate battery has a uniform distribution of C, O, F, and P—common components of SEI associated with LP30 electrolyte^[48]—with almost no transition metal signal, while the normal battery has high concentrations of C, O, F, P, and additional signal from Ni, Mn, and Co in the thicker regions of the SEI. The elemental survey of the iongate battery anode detects at most 0.03 at% of any transition metal (Figure 4c) whereas the normal battery has ≈ 2 at% of the SEI composed of transition metals in a nearly exact ratio of 5:3:2 (Ni:Mn:Co) that agrees with the cathode chemistry (Figure 4f). Full elemental survey data can also be found in Figure S12 in the Supporting Information. Clearly the iongate effectively suppresses transition metal ion crossover

and dramatically improves SEI formed at these elevated temperatures and during long periods of storage time.

Last, the iongate separator shut-off performance was evaluated in an iongate battery configuration (Figure 5). Again, to ensure the iongate was in a fully oxidized state before battery cycling the iongate separator underwent cyclic voltammetry and a 30 min oxidation hold at 3.6 V, as performed in Figures 3 and 4. Cycling of the cell with the iongate separator in the “on” state shows performance similar to a conventional cell at charging rates of C/10, C/5, and C/3 (Figure 5a). All discharge rates were maintained at C/10. However, when the iongate separators are reduced at 2.2 V for 30 min and cycling is resumed, negligible capacity is achieved at C/3, effectively resulting in complete battery shut-off due to large polarization of >1 k Ω . This is reflected in the cell impedance rise measure by EIS in Figure 5b. The spectra were best fitted with an equivalent circuit as shown in Figure S13 in the Supporting Information with 3 RC elements correspond to the cathode, the anode, and the iongate separator, respectively. Fitting results show a large increase of nearly 10 \times in the resistive element of the iongate component, which matches well with the results seen in DC measurements. This indicates that the iongate in the “off” state shows a dramatically reduced rate for ion transport. This observation is further supported by EIS measurements of the iongate separator as the working electrode (Figure S14, Supporting Information), which most notably shows a huge increase (nearly two orders of magnitude) in the Warburg diffusion tail element when the material is reduced, denoting the reduced rate of diffusion

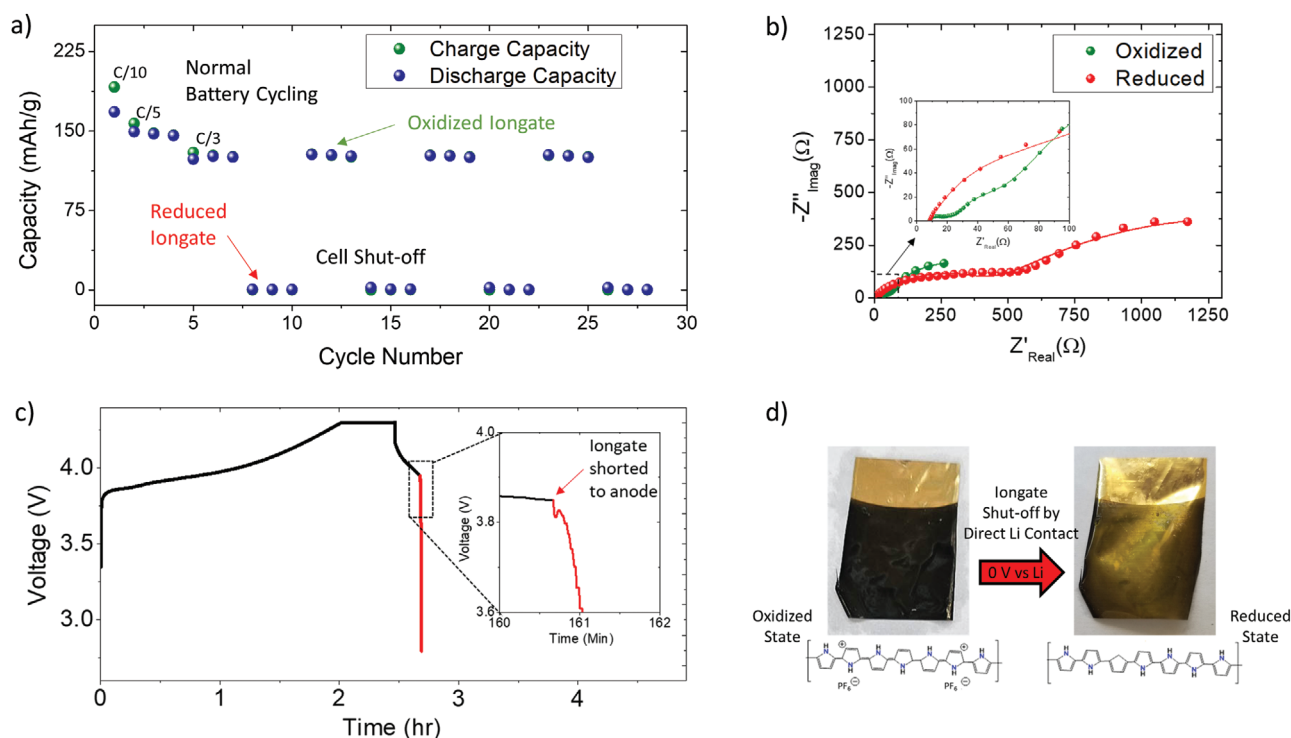


Figure 5. a) Cycling and ex operando switching capacity profile of an Li/iongate/NMC cell showing similar performance to a conventional cell while the iongate is in the oxidized “on” state, but cell shut-off while the iongate is in the reduced “off” state. The dots are measured data points and the lines are fitted results. b) Full cell EIS spectra showing the cell resistance difference between the two iongate redox states. c) Voltage profile of rapid in operando cell shut-off achieved by directly shorting the iongate separator electrode to the Li anode. d) Optical images showing iongate color change after direct shorting at 0 V to the Li anode.

processes within the iongate material. It is this decrease in diffusion rate in the iongate material itself that translates to the switching performance observed in the full cell.

Additionally, a cycling stability test was performed comparing a normal cell without the iongate separator to a cell with an iongate separator that was kept in the oxidized state throughout the entirety of cycling. The addition of the iongate has a negligible effect on cell capacity and cycling stability although there is an increase in cell resistance (Figure S15, Supporting Information).

While 30 min potential holds were applied to the iongate to ensure full oxidation or reduction during most of our experiments, due to the pseudocapacitive nature of PPy as an electrode material, the majority of switching capacity is achieved in a matter of seconds (Figure S16, Supporting Information). Considering this rapid oxidation state switching of the iongate, in situ shut-off of the cell was investigated by directly shorting the iongate separator to the anode during discharge of the battery (Figure 5c). By externally shorting the iongate separator to the 0 V Li anode, rapid reduction occurs with concurrent increase in overall cell impedance. This in turn results in cell shut-off as the discharge voltage rapidly decayed to the 2.7 V lower cut-off limit. The inlay of the discharge voltage profile highlights the moment the iongate is shorted and the fall in cell voltage, where this process only takes tens of seconds. Postmortem optical image of the reduced iongate separator shows a clear color change from the original darker oxidized state to a yellowish hue indicating that the direct contact with Li has indeed fully reduced the entire separator to an “off” state (Figure 5d). This color change is to be expected as PPy is a well-known electrochromic material,^[49] marking an effective safety mechanism during failure events such as Li dendrite penetration or mechanical deformation that would short the iongate to the anode.

3. Conclusion

In summary, we have developed an ultrathin (300 nm) polypyrrole/polydopamine (PPy:PDA) iongate membrane coated directly on a conventional Celgard separator that is capable of rapid and reversible switching of its ionic conductivity. The iongate separator maintains flexibility and displays improved wettability. A switching ratio of 10 \times was achieved between its oxidized “on” state and reduced “off” state. This iongate separator represents a novel approach to battery safety and control by allowing dynamic control of the separator ionic conductivity and overall ion flux. When storing a battery with the iongate separator in the reduced “off” state, ion flux can be dramatically suppressed. The iongate battery showed \approx 37% reduction in capacity loss versus a normal cell and nearly completely eliminated transition metal (Ni, Mn, Co) crossover when stored at 55 °C for 2 weeks. The iongate battery also displays cycling performance similar to a normal battery while in the “on” state, but effectively shuts-off of the cell when the iongate is reduced to the “off” state. Furthermore, the iongate can be turned off by directly shorting it to the lithium anode, pointing to its potential as a safety mechanism in the event of an internal short. Improvements to performance still remain, but there is an extensive library of conducting polymer materials with similar

properties that show great promise for future development of iongate separators for battery and other electrochemical storage applications.

4. Experimental Section

Au Sputter Coating Celgard: Celgard 2400 was cut into large square (10 cm \times 10 cm) and gently cleaned with ethanol and Kimwipe to remove any dust and other surface contaminants. These squares of Celgard were then placed into the vacuum chamber of a Ladd/Hummer 6.2 sputter coat machine equipped with a 99.999% Au target and Ar gas. The vacuum chamber was evacuated to 80 mTorr with a steady flow of Ar and 7 min of sputter coating was performed at a current of 20 mA. This resulted in an \approx 10 nm Au coating on the surface of the Celgard estimated according to the standard deposition rates for the system published by the manufacturer.

Distillation and Purification of Pyrrole: The pyrrole monomer was purified before each deposition using a simple distillation process. The purified pyrrole solution appeared clear and was stored in a refrigerator in a sealed vial under an Ar blanket to prevent oxidation in ambient air.

Iongate Deposition Solution: The deposition solution was 0.1 M pyrrole and 0.05 M dopamine for the 2:1 ratio (for other ratios, the pyrrole concentration remained 0.1 M and dopamine was altered), and 0.1 M LiClO₄ or 0.1 M LiTFSI all dissolved in 18 m Ω water prepared by reverse osmosis. This solution was stirred for at least 10 min to ensure a well-mixed solution.

Iongate Deposition Process: The Au-coated Celgard was connected to Gamry Interface 1000 potentiostat as the working electrode, a stainless-steel shim as the counter electrode, and a Ag/AgCl electrode as the reference. These were secured in place parallel to each other and dipped into the deposition solution so that about 6 cm of the Celgard was submerged and 4 cm was left as exposed Au. To improve deposition quality, the deposition solution was slightly stirred (magnetic stir bar at 300 RPM) and cooled using an ice bath to reach a temperature below 5 °C.

To electropolymerize the PPy:PDA onto the Au-coated Celgard, a constant potential of 0.65 V (vs Ag/AgCl) was applied. The deposition time determined the thickness of the iongate membrane and 180 s results in the 300 nm LiTFSI-doped membrane.

The deposited iongate separators were removed from the solution and rinsed in a di-ionized water bath three times to remove excess monomers and salt. They were dried overnight before assembling into other electrochemical cells.

XPS Characterization: XPS spectra (Figure S10, Supporting Information) used to calculate the doping level of iongate material were performed by a PHI Quantera SXM, Scanning X-ray Microprobe and was carried out using Al anode source at 15 kV and all the peaks were fitted based on the reference C–C bond at 284.6 eV. All XPS measurements were collected with a 300 mm \times 700 mm spot size using a charge neutralizer during acquisition. Survey scans were collected with a 1.0 eV step size, and were followed by high resolution scans with a step size of 0.05 eV for N1s regions.

Li/Iongate/Li Cell Setup: A symmetric three-electrode pouch cell was used to measure iongate across membrane performance as seen in Figure 3. Two 15 mm diameter disks of Li were pressed onto Cu foil and a Ni tab was taped to the backside as a current collector. The iongate separator was placed between the Li disks and an additional pristine Celgard separator was used to prevent the exposed PPy:PDA membrane from contacting the Li metal. An additional Al tab was taped to the exposed Au-coated Celgard to provide electrical contact to the iongate separator. The entire cell was filled with LP 30 (1 M LiPF₆ in 1:1 EC:DMC), or other electrolyte, and sealed using an MTI vacuum sealer within a Ar filled glovebox.

CV and the potentiostatic voltage holds to switch the redox states were performed using the iongate separator/Au contact as the working electrode and the Li electrode 1 as the counter and reference electrodes. The CV was performed at 10 mV s⁻¹ sweeping between 2.2 and 3.8 V and

the voltage holds to reduce and oxidized the iongate were performed at 2.2 and 3.8 V for 30 min to ensure full switching. The working electrode was then disconnected from the iongate separator and switched to Li electrode 2. Across membrane DC galvanostatic testing and AC impedance were performed immediately after the end of the iongate switching voltage holds. ± 1 mA (0.57 mA cm⁻²) was applied for the DC measurement and AC impedance was acquired between 7 MHz to 10 mHz at open circuit potential.

Li/Iongate/NMC Pouch Cell Parameters and Testing: Small pouch cells were assembled with the iongate separator between a Li metal anode and NMC532 (Li_xNi_{0.5}Mn_{0.3}Co_{0.2}O₂) cathode and used for testing results shown in Figures 4 and 5. The cathode had a capacity of 2.2 mAh cm⁻² and contained NMC532, carbon nanotubes, and polyvinylidene fluoride in a mass ratio of 97.5:1:1.5 on Al foil (Hunan Hong Xiang New Energy Technology Co., Ltd.). These were cut into 1.77 cm² disks and contacted with an Al tab tapped to the back. The anode current collector was a copper sheet with a Ni tab tapped to the back. 500 μ m thick Li disk with an area of 2.27 cm² was rolled onto the surface of the Cu inside of an Ar glovebox (O₂ < 1 ppm, H₂O < 1 ppm). The iongate separator area was at least 4.2 mm \times 4.2 mm to ensure full coverage of the active area with an additional pristine Celgard to prevent physical contact with the electrode. An Al tab was pressed and tapped directly to an area exposed Au that was outside of the active material area. The laminated pouch cell was sealed using an MTI MSK-115A-S vacuum sealer in an argon filled glove box after ≈ 0.5 mL of electrolyte (excess) was added. Parafilm and plexiglass sheets were used to apply pressure to the cell and iongate contact with spring-loaded clamps.

Supporting Information

Supporting Information is available from the Wiley Online Library or from the author.

Acknowledgements

Funding for this project was provided by LG Chem through the Global Innovation Contest. The majority of cell fabrication and electrochemical testing was performed in the UCSD-MTI Battery Fabrication and the UCSD-Arbin Battery Testing Facility. The authors acknowledge Hunan Hong Xiang New Energy Technology Co., Ltd. for supplying high capacity NMC cathode tapes.

Conflict of Interest

The authors declare no conflict of interest.

Author Contributions

P.L. proposed the idea and directed the research along with Z.C. and H.L. All the authors contributed to the planning, materials fabrication, experimental design and analysis, and manuscript preparation. M.S.G. performed the majority of separator fabrication and characterization as well as cell fabrication and electrochemical testing. Q.Y., M.L., and Z.W. aided in characterization and cell design. J.H. and H.Z. helped in experimental design and analyzing the results. S.K. helped develop initial PPY deposition process.

Data Availability Statement

The data that support the findings of this study are available in the Supporting Information of this article.

Keywords

battery safety, battery shut-off, battery storage, iongate separators, smart separators

Received: March 5, 2021

Revised: April 23, 2021

Published online:

- [1] J. A. McAllister, A. E. Farrell, *Energy* **2007**, *32*, 1177.
- [2] W. Cole, A. Frazier, *Cost Projections for Utility-Scale Battery Storage: 2020 Update*, National Renewable Energy Lab. (NREL), Golden, CO **2020**.
- [3] Lithium-ion Batteries-Market Report, <https://roskill.com/market-report/lithium-ion-batteries/> (accessed: February 2021).
- [4] T. Markel, presented at MIT Energy Initiative Transportation Electrification Symp., Cambridge, MA, April **2010**.
- [5] B. Kroposki, G. Martin, in *IEEE PES General Meeting* **2010**, pp. 1–4, <https://doi.org/10.1109/PES.2010.5589753>.
- [6] M. R. Palacín, A. de Guibert, *Science* **2016**, *351*, 1253292.
- [7] S.-M. Bak, E. Hu, Y. Zhou, X. Yu, S. D. Senanayake, S.-J. Cho, K.-B. Kim, K. Y. Chung, X.-Q. Yang, K.-W. Nam, *ACS Appl. Mater. Interfaces* **2014**, *6*, 22594.
- [8] T. Bowen, I. Chernyakhovskiy, P. Denholm, Grid-Scale Battery Storage: Frequently Asked Questions, <https://www.nrel.gov/docs/fy19osti/74426.pdf> (accessed: February 2021).
- [9] L. Zhou, Y. Zheng, M. Ouyang, L. Lu, *J. Power Sources* **2017**, *364*, 242.
- [10] W. Seong, K.-Y. Park, M. Lee, S. Moon, K. Oh, H. Park, S. Lee, K. Kang, *Energy Environ. Sci.* **2018**, *11*, 970.
- [11] G. Pistoia, A. Antonini, R. Rosati, D. Zane, *Electrochim. Acta* **1996**, *41*, 2683.
- [12] A. Blyr, C. Sigala, G. Amatucci, D. Guyomard, Y. Chabre, J.-M. Tarascon, *J. Electrochem. Soc.* **1998**, *145*, 194.
- [13] W. Li, J. Hicks-Garner, J. Wang, J. Liu, A. Gross, E. Sherman, J. Graetz, J. Vajo, P. Liu, *Chem. Mater.* **2014**, *26*, 3403.
- [14] I. Bauer, M. Kohl, H. Althues, S. Kaskel, *Chem. Commun.* **2014**, *50*, 3208.
- [15] H. Maleki, J. N. Howard, *J. Power Sources* **2009**, *191*, 568.
- [16] P. Sun, R. Bisschop, H. Niu, X. Huang, *Fire Technol.* **2020**, *56*, 1361.
- [17] C. Negroni, Boeing Dreamliner's Lithium-Ion Battery Fails On United Flight To Paris, <https://www.forbes.com/sites/christinene-negroni/2017/12/01/dreamliners-beleaguered-lithium-ion-battery-creates-problem-on-united-flight-to-paris/> (accessed: February 2021).
- [18] D. J. Noelle, M. Wang, A. V. Le, Y. Shi, Y. Qiao, *Appl. Energy* **2018**, *212*, 796.
- [19] Q. Wang, P. Ping, X. Zhao, G. Chu, J. Sun, C. Chen, *J. Power Sources* **2012**, *208*, 210.
- [20] M. Wang, A. V. Le, Y. Shi, D. J. Noelle, Y. Qiao, *Appl. Phys. Lett.* **2017**, *110*, 083902.
- [21] Z. Chen, P.-C. Hsu, J. Lopez, Y. Li, J. W. F. To, N. Liu, C. Wang, S. C. Andrews, J. Liu, Y. Cui, Z. Bao, *Nat. Energy* **2016**, *1*, 15009.
- [22] P. Yan, Y. Zhu, X. Pan, H. Ji, *Int. J. Energy Res.* **2021**, *45*, 2776.
- [23] Y. E. Hyung, D. R. Vissers, K. Amine, *J. Power Sources* **2003**, *119–121*, 383.
- [24] B. Wu, F. Pei, Y. Wu, R. Mao, X. Ai, H. Yang, Y. Cao, *J. Power Sources* **2013**, *227*, 106.
- [25] X. Li, W. Li, L. Chen, Y. Lu, Y. Su, L. Bao, J. Wang, R. Chen, S. Chen, F. Wu, *J. Power Sources* **2018**, *378*, 707.
- [26] J. R. Dahn, J. Jiang, L. M. Moshurchak, M. D. Fleischauer, C. Buhrmester, L. J. Krause, *J. Electrochem. Soc.* **2005**, *152*, A1283.

- [27] J. Ding, T. Tian, Q. Meng, Z. Guo, W. Li, P. Zhang, F. T. Ciacchi, J. Huang, W. Yang, *Sci. Rep.* **2013**, *3*, 2485.
- [28] T.-H. Yu, *EP0951080A1*, **1999**.
- [29] H. Wu, D. Zhuo, D. Kong, Y. Cui, *Nat. Commun.* **2014**, *5*, 5193.
- [30] M. S. Gonzalez, Q. Yan, J. Holoubek, Z. Wu, H. Zhou, N. Patterson, V. Petrova, H. Liu, P. Liu, *Adv. Mater.* **2020**, *32*, 1906836.
- [31] C. Deslouis, T. El Moustafid, M. M. Musiani, B. Tribollet, *Electrochim. Acta* **1996**, *41*, 1343.
- [32] P. Burgmayer, R. W. Murray, *J. Phys. Chem.* **1984**, *88*, 2515.
- [33] C. Weidlich, K.-M. Mangold, *Electrochim. Acta* **2011**, *56*, 3481.
- [34] M. E. Abdelhamid, A. P. O'Mullane, G. A. Snook, *RSC Adv.* **2015**, *5*, 11611.
- [35] Z. Wang, R. Pan, C. Ruan, K. Edström, M. Strømme, L. Nyholm, *Adv. Sci.* **2018**, *5*, 1700663.
- [36] X.-W. Gao, Y.-F. Deng, D. Wexler, G.-H. Chen, S.-L. Chou, H.-K. Liu, Z.-C. Shi, J.-Z. Wang, *J. Mater. Chem. A* **2014**, *3*, 404.
- [37] F.-H. Du, B. Li, W. Fu, Y.-J. Xiong, K.-X. Wang, J.-S. Chen, *Adv. Mater.* **2014**, *26*, 6145.
- [38] L. Qie, L.-X. Yuan, W.-X. Zhang, W.-M. Chen, Y.-H. Huang, *J. Electrochem. Soc.* **2012**, *159*, A1624.
- [39] C. Wang, W. Zheng, Z. Yue, C. O. Too, G. G. Wallace, *Adv. Mater.* **2011**, *23*, 3580.
- [40] T. Patois, B. Lakard, S. Monney, X. Roizard, P. Fievet, *Synth. Met.* **2011**, *161*, 2498.
- [41] H. Lee, S. M. Dellatore, W. M. Miller, P. B. Messersmith, *Science* **2007**, *318*, 426.
- [42] W. Zhang, F. Yang, Z. Pan, J. Zhang, B. Zhao, *Macromol. Rapid Commun.* **2014**, *35*, 350.
- [43] K. Semin, L. Jang, H. Park, J. Y. Lee, *Sci. Rep.* **2016**, *6*, 30475.
- [44] S. J. An, J. Li, C. Daniel, S. Kalnaus, D. L. Wood, *J. Electrochem. Soc.* **2017**, *164*, A1755.
- [45] J. Shim, R. Kosteki, T. Richardson, X. Song, K. A. Striebel, *J. Power Sources* **2002**, *112*, 222.
- [46] B. A. Johnson, R. E. White, *J. Power Sources* **1998**, *70*, 48.
- [47] P. Bai, J. Li, F. R. Brushett, M. Z. Bazant, *Energy Environ. Sci.* **2016**, *9*, 3221.
- [48] R. May, Y. Zhang, S. R. Denny, V. Viswanathan, L. E. Marbella, *Cell Rep. Phys. Sci.* **2020**, *1*, 100239.
- [49] P. Camurlu, *RSC Adv.* **2014**, *4*, 55832.